

## Effect of synthesis temperature on Al-substituted $\alpha$ -Ni(OH)<sub>2</sub> as Cathode Material for zinc-nickel battery

Ming-jun Xie<sup>1</sup>, Hong-wei Guan<sup>2</sup>, Yu-ting Fu<sup>3</sup>, Han Wu<sup>1</sup>, Yan Zhao<sup>1\*</sup>, Jian-jun Guan<sup>1</sup>, Peng Gao<sup>1</sup>

<sup>1</sup> School of Mechanical Engineering, Liaoning Petrochemical University, Fushun 113001, Liaoning, China

<sup>2</sup> Guangzhou HEMTEC Environmental Technology Co., Ltd. Guangzhou, 510610, China

<sup>3</sup> School of Environmental & Safety Engineering, Liaoning Petrochemical University, Fushun 113001, Liaoning, China

\*E-mail: [zhaoyan@lnpu.edu.cn](mailto:zhaoyan@lnpu.edu.cn)

Received: 8 September 2021 / Accepted: 27 October 2021 / Published: 27 December 2022

---

Al-substituted  $\alpha$ -Ni(OH)<sub>2</sub> cathode material was synthesized by buffer solution method at different temperatures (T=15°C, 35°C, 55°C, 75°C). The morphology and crystalline structure of Ni(OH)<sub>2</sub> were characterized by SEM and XRD. The electrochemical properties were tested by CV cyclic voltammetry and constant current charge and discharge. The results show that different synthesis temperatures of the electrode significantly affect the electrochemical properties. When the preparation temperature at 15°C or 35°C,  $\beta$ -Ni(OH)<sub>2</sub> and  $\alpha$ -Ni(OH)<sub>2</sub> phase exist together but at higher temperatures of 55°C and 75°C, the samples are pure  $\alpha$ -phase. Moreover, the polarization degree of the electrode was minimum with the best electrochemical properties at the synthesis temperature of 55 °C. After 55 cycles in the single-flow zinc-nickel battery, the specific capacity was stable at 310mAh/g, and the attenuation rate was 1.6%, which was better than the other four samples under the same conditions (T =15°C) 6.9%, (T=75°C) 4.3% and (T=35°C) 2.6%, ( $\beta$ - Ni(OH)<sub>2</sub>) 11.16%

---

**Keywords:** buffer solution method, cyclic voltammetry, constant current charge and discharge, the specific capacity, single-flow zinc-nickel battery

### 1. INTRODUCTION

As environmental pollution increases, there is an increasing focus on clean energy and energy storage devices. As a traditional aqueous solution battery, the nickel-zinc battery is environmentally friendly and pollution-free. It has the advantages of safety, low cost, and high power, so it is not only regarded as a substitute for traditional nickel-cadmium batteries and lead-acid batteries, but also regarded as lithium Alternatives to ion battery [1-2]. The potential of electrode material Ni(OH)<sub>2</sub> for improving battery performance has attracted wide attention in recent years. Bode has found in his crystal theory [3] that nickel hydroxide is usually an apple green powder with two crystal structures,  $\alpha$ -Ni(OH)<sub>2</sub> and  $\beta$ -

$\text{Ni(OH)}_2$ . After it was charged, the oxidized state of  $\text{NiOOH}$  after charging corresponds to  $\gamma\text{-NiOOH}$  and  $\beta\text{-NiOOH}$  [4] respectively, while the electrochemical performance of  $\alpha$ -form is usually better than that of  $\beta\text{-Ni(OH)}_2$ . The theoretical specific capacity of  $\beta\text{-Ni(OH)}_2$  is 289mAh/g, which is stable and can only exchange at most one electron during the charging and discharging process. In contrast,  $\alpha\text{-Ni(OH)}_2$  exchanges more than one electron, up to 1.67 electrons, during the charging and discharging process. The theoretical specific capacity of  $\alpha\text{-Ni(OH)}_2$  is 482mAh/g, which is about 1.5 times that of  $\beta\text{-Ni(OH)}_2$ , and  $\alpha\text{-Ni(OH)}_2$  has better redox reversibility and discharge potential platform. However,  $\alpha\text{-Ni(OH)}_2$  is a metastable phase that is easily converted to  $\beta\text{-Ni(OH)}_2$  during synthesis [5-6]. Much work has focused on the use of (Al[7-9], Co[10,11], Fe[12], Mn[13] and Zn[14]) to partial substitution nickel ions in the nickel hydroxide lattice in order to stabilize  $\alpha\text{-Ni(OH)}_2$ . Since the substitution element does not participate in the electrochemical oxidation-reduction reaction, the limited capacity and energy density usually decrease with the increase of the substitution rate. Al ions is the most attractive of these metal ions due to its high stability in the trivalent state and low cost. The electrolyte used in alkaline secondary batteries is usually a concentrated alkaline aqueous solution and Al ions is easily dissolved in the concentrated alkaline electrolyte. Yin-Mei Wan [15] studied the properties of  $\text{Ni(OH)}_2$  materials at different electrodeposition temperatures and found that temperature had a significant effect on crystalline structure, morphology, specific surface area and electrochemical properties. Chang-Jiu Lin [16] investigated the performance of  $\text{Al}^{3+}$  doped  $\alpha\text{-Ni(OH)}_2$  composite CNTs electrode materials at high temperatures used chemical precipitation method. He found that high temperatures stabilize the  $\text{Ni(OH)}_2$  structure to improve charging and discharging efficiency and inhibit oxygen precipitation effectively. Yan-Wei Li's [17] team found that nickel hydroxide powders synthesized at high temperatures (40~60°C) would form crystalline  $\beta$ -nickel hydroxide, while at low temperatures (0~20°C) would induce precipitation of crystalline nickel hydroxide badly.

According to previous studies, the properties of  $\text{Ni(OH)}_2$  can be improved with the reaction temperature. In this paper, we used buffer solution method to investigate the electrochemical properties of Al-substituted  $\alpha\text{-Ni(OH)}_2$  at different synthesis temperatures. The buffered solution method can stabilize the pH of the solution and thus enhance the physicochemical properties of the sample. In this study, four temperatures ( $T=15^\circ\text{C}$ ,  $35^\circ\text{C}$ ,  $55^\circ\text{C}$  and  $75^\circ\text{C}$ ) were used to synthesis Al-substituted  $\alpha\text{-Ni(OH)}_2$  and  $\beta\text{-Ni(OH)}_2$  was also added for performance comparison.

## 2. EXPERIMENTAL

### 2.1 The electrolyte configuration

Dissolved 280.55 g of KOH completely in 350 ml of distilled water then add 40.71g ZnO and 10g LiOH until the solution becomes clear.

### 2.2 Al-substituted $\alpha\text{-Ni(OH)}_2$ synthesis

Dissolved 5.4g of ammonium chloride solid in a small amount of distilled water, then added 35 mL of concentrated ammonia and dilute the solution to 100 mL, pH = 10.0, thus completed the preparation of  $\text{NH}_3\text{-NH}_4\text{Cl}$  buffer solution.

22.08gNiSO<sub>4</sub>·6H<sub>2</sub>O, 5.10gAl(NO<sub>3</sub>)<sub>3</sub>·9H<sub>2</sub>O were dissolved in 200mL deionized water, where the molar ratio of Ni to Al was 14:86. Then 11.2 g of NaOH, 6.4 g of anhydrous sodium carbonate solids were dissolved in 200 mL of deionised water. Finally, these two solutions were gradually added to the beaker containing the buffer solution at 5mL/min under magnetic stirring, the reaction temperature was set to 15°C, 35°C, 55°C and 75°C respectively, this mixture was reacted under strong stirring for 5 hours and the final mixture was aged at 60°C for 8 hours, then filtered and washed with heated deionised water and the resulting solid was dried in a vacuum drying oven to a constant weight. The constant weight solid was placed in a ball mill jar, an appropriate amount of stainless balls were added and the ball mill was used to mill the powdered sample at 40r/min for 4h.

### 2.3 Preparation of electrodes

The active substance (Ni(OH)<sub>2</sub>, 60%), graphite emulsion (20%) and nickel powder (20%) are mixed and ground into a slurry by adding C<sub>2</sub>H<sub>6</sub>O in an agate mortar for 30 minutes. Scrape the slurry on one side of a 2cm×2cm piece of foamed nickel, sandwich it between two pieces of nickel foam and dried in a vacuum drying oven at 60°C for 4 hours. Finally, the electrodes were made by pressing the tablets on a powder press at 20 MPa (Ni(OH)<sub>2</sub> loading of about 10 mg/cm<sup>2</sup>). Commercially β-Ni(OH)<sub>2</sub> was used as a comparison electrode.

The active substance (Ni(OH)<sub>2</sub>, 60%), graphite emulsion (20%) and nickel powder (20%) are mixed, added with the appropriate amount of anhydrous ethanol and ground in an agate mortar for 30 minutes, after grinding into a slurry, the slurry is scraped onto one side of a 2cm x 2cm piece of nickel foam with a scraper, and the coating was sandwiched between the two pieces of nickel foam with another piece of the same size before being placed in a vacuum dry in a vacuum oven at 60°C for four hours. Finally, the electrodes (Ni(OH)<sub>2</sub> loading of approximately 10 mg/cm<sup>2</sup>) were compressed on a powder press at a pressure of 20 MPa. Commercially available β-Ni(OH)<sub>2</sub> was used for the reference.

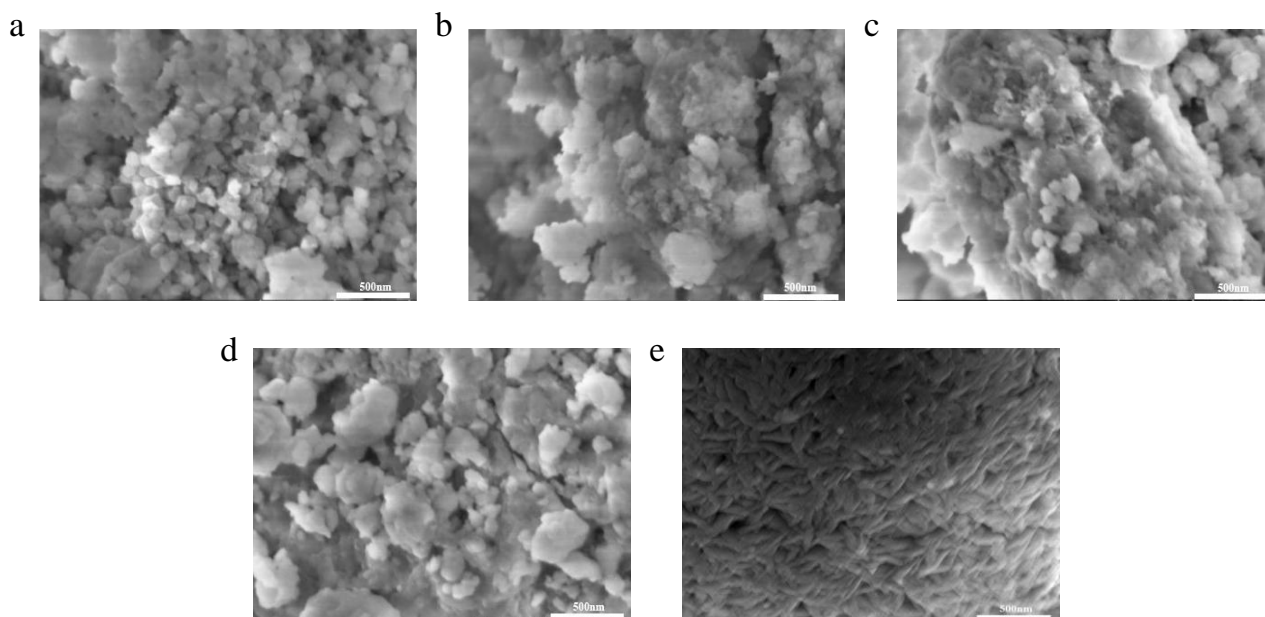
### 2.4 Characterization

SEM was carried out with a ZEISS MERLIN COMPACT scanning electron microscope and the XRD analysis of the synthesis cathode material was carried out using a D/Max-3B X-ray diffractometer manufactured in Japan with the following parameters: operating voltage of 40 KV, operating current of 30 mA, divergence slit width of 1°, anti-divergence slit of 1 ° and acceptance slit of 0.3 °. Cu-Kα was used as the radiation source, the sampling spacing was 0.02 °, the scanning range was 0-90 °, and the scanning speed was 5.0 °/min.

This experiment was carried out at the CHI000B electrochemical workstation for cyclic voltammetry testing of the battery. The three-electrode test system for testing, with a mercury oxide electrode as reference electrode (SEC), the scanning rate was 0.5mV/s and scanning voltage was 0~0.7V. The battery test system was carried out on GN-CD30V10A at a 100mA/g current for constant current charge and discharge experiments. The voltage was at 1.2V~2.2V and the electrode material was vacuum dipped for more than 3h during the current activation and test section. The β-Ni(OH)<sub>2</sub> was also tested under the same conditions.

### 3. RESULTS and DISCUSSION

#### 3.1 SEM



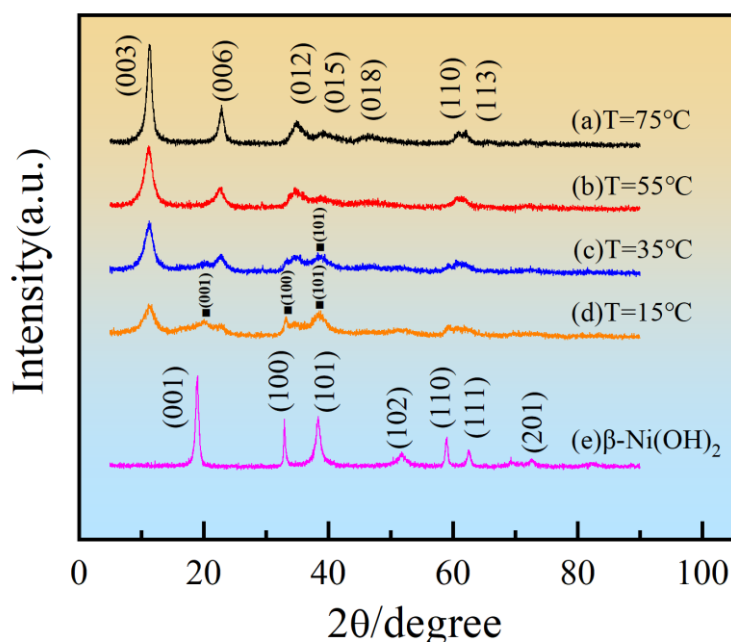
**Figure 1.** SEM diagrams of  $\beta$ -Ni(OH)<sub>2</sub> and  $\alpha$ -Ni(OH)<sub>2</sub>, (a) 15°C, (b) 35°C, (c) 55°C, (d) 75°C, (e)  $\beta$ -Ni(OH)<sub>2</sub>.

Figure 1 shows the SEM images of  $\alpha$ -Ni(OH)<sub>2</sub> at different synthesis temperatures ( $\times 50000$ ), which clearly shows that the synthesis temperature has a great influence on the morphology of the sample. Part of the agglomeration phenomenon occurred in the sample of Ni(OH)<sub>2</sub> at 15°C. The agglomeration will reduce the surface area of the reaction, and the more particles agglomerated, the smaller the reaction area of the battery, thereby reducing the electrochemical performance of the sample. The sample at 35°C has a certain agglomeration, compared with the sample at 15°C, there is no obvious particle phenomenon. Relatively speaking, the effect on the surface area of the reaction will be smaller, and cracks will increase the surface area of the reaction. In the 55 °C sample, the particles are rough, with pores on the surface, and the agglomeration almost disappears, which is conducive to improving the specific capacity, cycling stability of the cell. The agglomeration phenomenon reappears at 75°C. The SEM images of the synthesized samples at each synthesis temperature show that the particle size of the samples first becomes larger and then smaller as the temperature rises.

#### 3.2 XRD

Figure 2 compares the XRD patterns of the  $\beta$ -Ni(OH)<sub>2</sub> and  $\alpha$ -Ni(OH)<sub>2</sub> synthesized at 15°C, 35°C, 55°C, and 75°C respectively. The position of the  $\alpha$ -Ni(OH)<sub>2</sub> diffraction peak is consistent with the standard pattern (JCPDS: 38-0715) as can be seen in the figure. The uniform precipitation of Al as an amphoteric metal in the Ni(OH)<sub>2</sub> lattice instead of dissolving in alkaline solution indicates that the synthesis of Al-substituted  $\alpha$ -Ni(OH)<sub>2</sub> in this experiment can be stable in alkaline solution. The Jade

software is used to compare and analyze the data of XRD. 4 kinds XRD of  $\alpha$ -Ni(OH)<sub>2</sub> samples show (003) crystallographic diffraction peaks in the low-angle region at  $2\theta$  of 12°, followed by (006) diffraction peaks near 22°. asymmetric diffraction peaks appear on the crystallographic planes at  $2\theta$  of 35° (012) and 39° (015), which are characteristic peaks due to the helical lamellar structure of  $\alpha$ -Ni(OH)<sub>2</sub>, and these diffraction peaks can be indexed to the hexagonal crystal system of cell characteristics. Although the samples are all in  $\alpha$ -phase structure, there are some differences between the samples at different temperatures.



**Figure 2.** XRD patterns of  $\beta$ -Ni(OH)<sub>2</sub> and  $\alpha$ -Ni(OH)<sub>2</sub> at different synthesis temperature: (a)75°C; (b)55°C; (c)35°C; (d)15°C; (e)  $\beta$ -Ni(OH)<sub>2</sub>.

The diffraction peaks of  $\beta$ -Ni(OH)<sub>2</sub> appeared at 20.06° and 38.52° when T=15°C (001)(100)(101), and also at 38.92° when T=35°C. When T=15°C, the diffraction peaks of  $\beta$ -Ni(OH)<sub>2</sub> (001)(100)(101) appear at 20.06° and 38.52°, and the sample at T=35°C also appears at 38.92° diffraction peak. In other words, the Al-substituted  $\alpha$ -Ni(OH)<sub>2</sub> synthesized at lower temperatures is a mixed phase with  $\alpha$  and  $\beta$ , but the sample is pure  $\alpha$  phase at higher temperatures of 55° and 75°. As the temperature increases, the intensity of the diffraction peak also increases significantly. The sharper the diffraction peak, the greater the relative intensity, the better the crystallinity of the crystal phase, and the better the quasi-reversibility of the electrochemical reaction, which is beneficial to improve the chemistry performance [18]. The sample at 15°C has the lowest peak value among the four Al-substituted  $\alpha$ -Ni(OH)<sub>2</sub> temperatures, so the specific discharge capacity will inevitably be affected. The relative intensity of the diffraction peaks of the samples at T=35°C, 55°C and 75°C is higher, and the half-height width is larger than that of  $\beta$ -Ni(OH)<sub>2</sub>. The wider the half-peak height and width, the smaller the microcrystalline size of the material [18], which tentatively verified that the size of the material synthesized in this experiment was relatively small. The differences in the diffraction peaks of these five samples indicated that the preparation temperature significantly affected the crystal structure of Ni(OH)<sub>2</sub>.

### 3.3 Cyclic Voltammetry

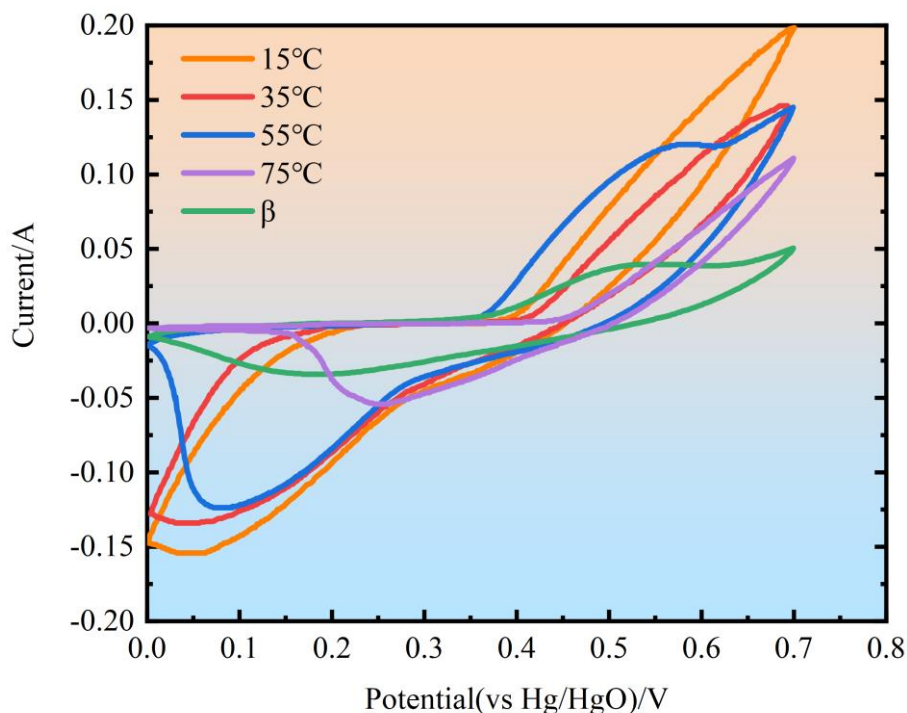


**Figure 3.** Cyclic voltammeter curves of Al-substituted  $\alpha$ -Ni(OH)<sub>2</sub> and  $\beta$ -Ni(OH)<sub>2</sub> electrode

In order to characterize the charging and discharging performance of the sample material electrodes, the degree of electrode reaction, reversibility and charging and discharging efficiency, cyclic voltammetry tests were carried out to simulate the charging and discharging process of the electrodes. The cyclic voltammetry curves and characteristic potentials are shown in Figure 3 and Table 1. The oxidation and reduction peaks of Al-substituted  $\alpha$ -Ni(OH)<sub>2</sub> and  $\beta$ -Ni(OH)<sub>2</sub> were single peaks for each temperature.

**Table 1.** The characteristic voltages of Al-substituted  $\alpha$ -Ni(OH)<sub>2</sub> and  $\beta$ -Ni(OH)<sub>2</sub> electrode

Samples	V <sub>a</sub> (V)	V <sub>c</sub> (V)	V <sub>a</sub> -V <sub>c</sub> (V)	Peak area
15°C	0.479	0.055	0.424	0.039
35°C	0.493	0.048	0.445	0.035
55°C	0.620	0.078	0.542	0.047
75°C	0.646	0.248	0.398	0.016
$\beta$ -Ni(OH) <sub>2</sub>	0.632	0.154	0.478	0.018

The peak current of the oxidation process of Al-substituted  $\alpha$ -Ni(OH)<sub>2</sub> sample electrode decreased with the increase of temperature, from 198mA at 15°C to 110mA at 75°C, while the peak current of  $\beta$ -Ni(OH)<sub>2</sub> was only 50mA, so it is obvious that the electrochemical performance of  $\alpha$ -Ni(OH)<sub>2</sub> is much better than that of  $\beta$ -Ni(OH)<sub>2</sub>.

The oxidation and reduction peaks of the Al-substituted  $\alpha$ -Ni(OH)<sub>2</sub> sample are shifted to higher potential, which means that its ability to accept charge is gradually getting stronger. As shown in Tab1, the difference between the oxidation and reduction potentials ( $\Delta E_p$ ) is related to the electrochemical reversibility. The larger  $\Delta E_p$  is, the more irreversible the electrochemical reaction is, which means that the polarization is also greater. The difference between the oxygen precipitation potential and oxidation peak potential of  $\beta$ -Ni(OH)<sub>2</sub> is smaller than that of  $\alpha$ -Ni(OH)<sub>2</sub>, which means that it is more difficult to precipitate oxygen at  $\alpha$ -Ni(OH)<sub>2</sub> electrode and the charging efficiency of the electrode will be higher. (T=15°C, 35°C, 55°C, 75°C), the integral areas of CV curves are 0.039, 0.035, 0.047, 0.016, 55°C Al-substituted  $\alpha$ -Ni(OH)<sub>2</sub> has the largest integral area, which means that the discharge specific capacity is the largest at 55°C, while the integral area of  $\beta$ -Ni(OH)<sub>2</sub> is only 0.018 is the smallest, and the discharge specific capacity is the worst. Therefore, an appropriate increase in the reaction temperature can effectively increase the oxygen precipitation overpotential to inhibit the precipitation of oxygen and effectively improve the charging and discharging efficiency of the electrode.

### 3.4 Constant current charge and discharge test

Fig4 shows the cycling performance curves of Al-substituted  $\alpha$ -Ni(OH)<sub>2</sub> and  $\beta$ -Ni(OH)<sub>2</sub> electrodes. The discharge capacities of  $\alpha$ -Ni(OH)<sub>2</sub> and  $\beta$ -Ni(OH)<sub>2</sub> increased gradually with the increase of cycling times. The highest discharge capacity was reached at about 15 cycles, and the discharge capacity at T=15°C, 35°C, 55°C and 75°C were higher than that of  $\beta$ -Ni(OH)<sub>2</sub>, where the lowest discharge capacity was 288mAh/g at T=15°C, but it was much higher than that of  $\beta$ -Ni(OH)<sub>2</sub>. The peak discharge capacity of the sample at 55°C was 320mAh/g, which was stabilized at 310mAh/g with the increase of the cycle number; the peak discharge capacity of the sample at 75°C was 310mAh/g and finally stabilized at 300mAh/g. From the 15th to the 55th cycle, the maximum capacity fade of  $\beta$ -Ni(OH)<sub>2</sub> was 11.16%, followed by (T=15°C) 6.9%, (T=75°C) 4.3%, (T=35°C) 2.6%, and (T=55°C) 1.6%. In sample preparation, temperature strongly affects the rate of precipitant generation, which in turn affects the stacking density of the resulting sample, and also changes the electrical conductivity. The Arrhenius equation [19] reaction temperature degree should increase by 1.4~1.5 times for every 10°C increase in the reaction rate, but at higher temperatures a side reaction occurs the effective concentration of NH<sub>3</sub> in the solution decreases instead, so the electrochemical properties decrease at 75°C instead.

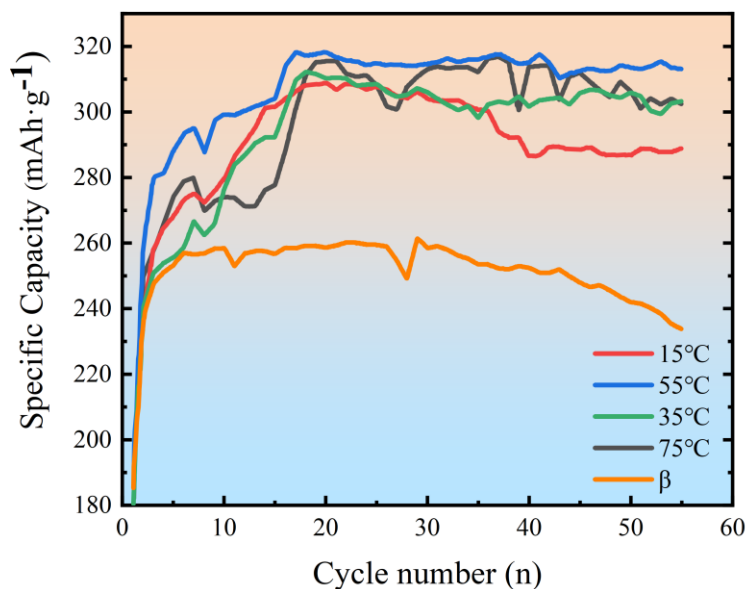


**Figure 4.** Cycle performance of Al-substituted  $\alpha$ -Ni(OH)<sub>2</sub> and  $\beta$ -Ni(OH)<sub>2</sub> electrode

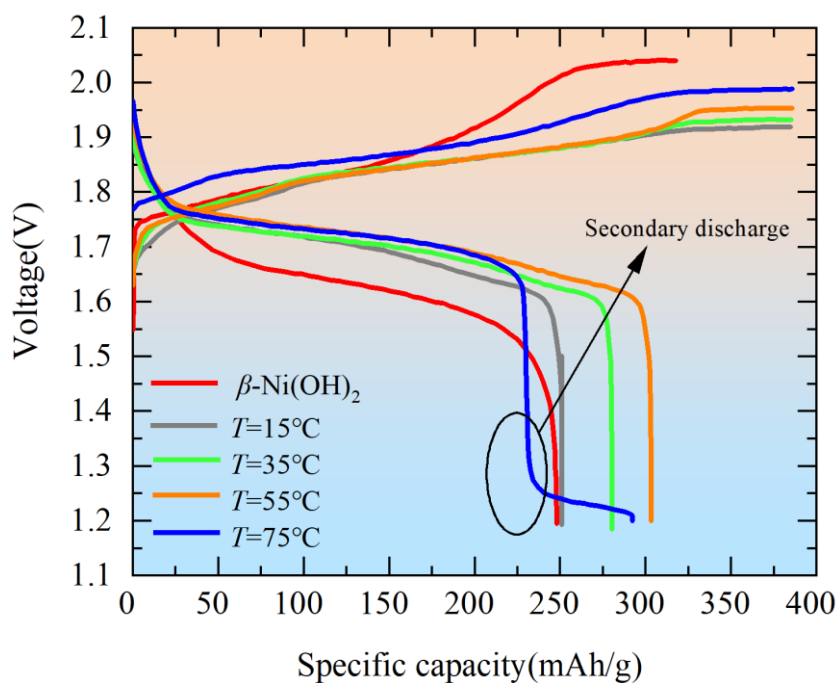


**Figure 5.** Charge-discharge curves of Al-substituted  $\alpha$ -Ni(OH)<sub>2</sub> and  $\beta$ -Ni(OH)<sub>2</sub> electrode

The charge and discharge curves of the five samples at 100mA/g shown in Fig5. When  $T=15^{\circ}\text{C}$ ,  $35^{\circ}\text{C}$  and  $55^{\circ}\text{C}$ , the discharge specific capacity increased with the increase of synthesis temperature as shown in Table 3, which are 251mAh/g, 280mAh/g and 303mAh/g, respectively. When  $T$  increases to  $75^{\circ}\text{C}$ , the discharge specific capacity decreases instead to 292mAh/g, while the  $\beta$ -Ni(OH)<sub>2</sub> discharge specific capacity was only 247mAh/g lower than the other samples. Tab3 calculates the maximum

number of electrons exchanged (NEE) of Ni atoms with the following formula, which more directly characterizes the electrochemical properties of the sample.

$$NEE = \frac{3600C_{exp}}{nF}$$

$C_{exp}$  (the maximum discharge specific capacity mAh/g);

$n$  (the molarity of Ni);

$F$  (Faraday's constant 96485.33C/mol);

$e = 1.60217663410 \times 10^{-19}C$

**Table 2.** Specific discharge capacity of different electrode materials

Reference	The electrode materials	The method of preparation	Discharge specific capacity(mAh/g)
Our work	Al doped $\alpha$ -Ni(OH) <sub>2</sub>	buffer solution	303
Xiao [13]	Mn-doped $\alpha$ -Ni(OH) <sub>2</sub>	buffer solution	302
Yao [21]	Al doped $\alpha$ -Ni(OH) <sub>2</sub>	buffer solution	294
Ren [20]	$\alpha$ -Ni(OH) <sub>2</sub> -Y(NO <sub>3</sub> )	urea decomposition	263
Li [17]	Al doped $\alpha$ -Ni(OH) <sub>2</sub>	chemical precipitation	250

**Table 3.** Electrochemical properties of samples

Samples	Middle discharge voltage(V)	Discharge capacity(mAh/g)	NEE
15°C	1.381	251	1.009e
35°C	1.381	280	1.127e
55°C	1.365	303	1.218e
75°C	1.533	292	1.173e
$\beta$ -Ni(OH) <sub>2</sub>	1.324	247	0.999e

The theoretical value of electron transfer in the two-phase conversion of  $\beta$ -Ni(OH)<sub>2</sub>/ $\beta$ -NiOOH is maximum 1. The discharge specific capacity of Al-substituted Ni(OH)<sub>2</sub> is determined by both its phase structure and the amount of inert element Al substitution, and the literature [22] reported that Al substitution forms the  $\alpha$ -crystalline phase, which makes the variable electron number of Ni(OH)<sub>2</sub> greater than 1~1.67, thus increasing the sample discharge specific capacity. The calculated results in Table 3 are consistent with this. The discharge specific capacity of the samples is the result of the action of the phase structure, and since  $\beta$ -Ni(OH)<sub>2</sub> has a better structural stability,  $\beta$  has a smaller discharge specific capacity compared to  $\alpha$  phase [22], so the smaller the maximum number of electrons of Ni atoms exchanged.

T=15°C, 35°C samples are mixed phases with the co-existence of  $\alpha$  and  $\beta$ , so the specific capacity decreases.

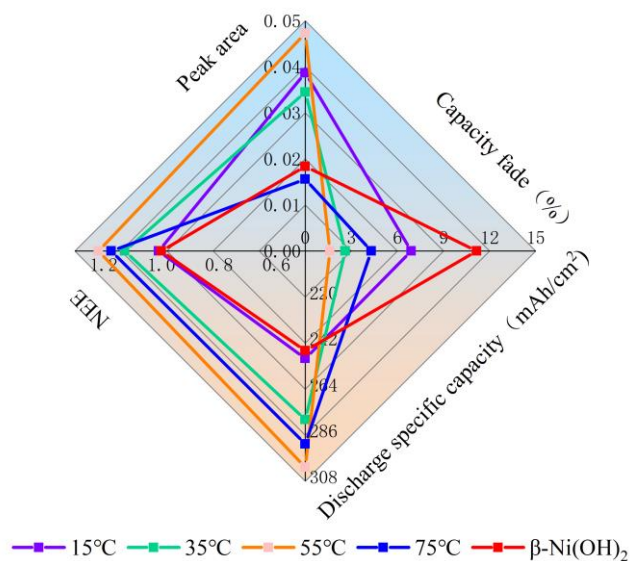


**Figure 6.** Comprehensive performance of Al-substituted  $\alpha$ -Ni(OH)<sub>2</sub> and  $\beta$ -Ni(OH)<sub>2</sub> electrode

The sample of T=55°C is pure  $\alpha$ -phase  $\alpha$ -Ni(OH)<sub>2</sub> with a small amount of water molecules between the layers, which facilitates the diffusion of proton H<sup>+</sup> during charging and discharging, so the specific capacity is slightly higher. The sample (T=75°C) 232mAh/g after the phenomenon of secondary discharge is shown in Figure 5, which may be in the sample while overcharging precipitation of oxygen led to partial loosening of some  $\alpha$ -Ni(OH)<sub>2</sub> in contact with nickel foam, with lower potential; while the contact with nickel foam precision  $\alpha$ -Ni(OH)<sub>2</sub> with higher potential thus leading to the discharge double platform phenomenon. The high temperature in the preparation may cause elemental segregation of Al<sup>3+</sup>, which converts  $\alpha$ -Ni(OH)<sub>2</sub> to  $\beta$ -Ni(OH)<sub>2</sub>, so the number of electrons exchanged is small at T=75°C. As is shown in Figure 6, changing the synthesis temperature can improve the cyclic performance and electrochemical stability of Al substituted  $\alpha$ -Ni(OH)<sub>2</sub>.

#### 4. CONCLUSION

In this paper, Al-substituted  $\alpha$ -Ni(OH)<sub>2</sub> cathode material was prepared by the buffer solution method at different synthesis temperatures T=15°C, 35°C, 55°C and 75°C.

(1) The synthesis temperature changed the morphology of  $\alpha$ -Ni(OH)<sub>2</sub> particles. With the increase of temperature in the particles first become smaller and then larger, at 55 °C, the particles are most dense.

(2) XRD shows that the samples at low temperature (T=15°C and 35°C) is mixed phases with  $\alpha$  and  $\beta$ . But when the samples at T=55°C and 75°C are pure  $\alpha$ -Ni(OH)<sub>2</sub>

(3) Cyclic voltammetry shows that changing the synthesis temperature appropriately can increase the oxygen precipitation overpotential to improve the charging and discharging efficiency of the electrode, and when  $T=55^{\circ}\text{C}$ , there is a larger peak area and peak current.

(4) The constant current charge/discharge experiment shows that the specific capacity of the sample increases and then decreases as the preparation temperature rises, and the maximum specific capacity (303mAh/g) is at  $T=55^{\circ}\text{C}$ . The capacity loss was only 1.6% after 55 cycles, while the discharge capacity (232mAh/g) became smaller at  $T=75^{\circ}\text{C}$ , and the capacity fade reached 4.3%.

#### ACKNOWLEDGMENT

This work was supported by Liaoning Province Department of Education Research Funding Project (NO. LJKZ0385) and Scientific Research Funds Project of Liaoning Education Department of China (No. L2019019).

#### References

1. J.F. Parker, I.R. Pala, C.N. Chervin, J.W. Long and D.R. Rolison, *J. Electrochem. Soc.*, 3(2016)163.
2. X.P. Gao and H.X. Yang, *Energy Environ Sci.*, 3(2010) 174.
3. H. Bode, T. Dehmelt and J. Witte, *Electrochim. Acta*, 11(1966) 1079.
4. A.K. Shukla, S. Venugopalan and B. Hariprakash, *J. Power Sources*, 100(2001)125.
5. V.G. Kumar, N. Munichandraiah, P.V. Kamath and A.K. Shukla, *J. Power Sources*, 56(1995)111.
6. P.V. Kamath, M. Dixit and J. Gopalakrishnan, *J. Electrochem. Soc.*, 146(1999)79.
7. K.T. Ehlssissen, A.D. Vidal, P. Genin, M. Figlarz and P. Willmann, *J. Mater. Chem.*, 3 (1993) 883.
8. P.V. Kamath, M. Dixit, L. Indira and A.K. Shukla, *J. Electrochem. Soc.*, 141 (1994) 2956.
9. Y.W. Li, J.H. Yao, C.J. Liu, W.M. Zhao, W.X. Deng and S.K. Zhong, *Int. J. Hydrogen Energy*, 35 (2010) 2539.
10. C. Faure, C. Delmas and P. Willmann, *J. Power Sources*, 36 (1991) 497.
11. Y. L. Zhao, J. M. Wang, H. Chen, T. Pan, J.Q. Zhang and C.N. Cao, *Electrochim. Acta*, 50 (2004) 91.
12. L. D. Guerlou and C. Delmas, *J. Power Sources*, 45 (1993) 281.
13. M. Xiao, F. Dou, S.G. Yao, R.Y. Xing, J. Cheng and Y.S. Yang, *Int. J. Electrochem. Sci.*, 15 (2020) 6024.
14. C. Tessier, L.G. Demourgues, C. Faure, A. Demourgues and C. Delmas, *J. Mater. Chem.*, 10 (2000) 1185.
15. Y. M. Wang, D.D. Zhao and Y.Q. Zhao, *RSC Adv.*, 2 (2012) 1074.
16. C.J. Liu, P.P. Li and L.H. Hang, *Adv. Mat. Res.*, 287(2011)1416.
17. Y.W. Li, Q.X. Yang and J.H. Yao, *Solid State Ionics*, 16 (2010) 221.
18. R. Cheary, E.D. Coelho and R.W. Cheary, *J. Appl. Crystallogr.*, 25 (2010)109.
19. C.H. Wang, J.W. Liang, J. Luo and J. Liu, *Sci. Adv.*, 7(2021)1896.
20. J.X. Ren, Z. Zhou, X.P. Gao and J. Yan, *Electrochim. Acta*, 52 (2006) 1120.
21. M. Xiao, R.Y. Xing, S.G. Yao, J. Cheng, Y.J. Shen and Y.S. Yang, *Int. J. Inorg. Mater.*, 34(2019)703.
22. Y.W. Li, J.H. Yao and Y.X. Zhu, *J. Power Sources*, 203(2012)177.